Inorg. Chem. **2006**, *45*, 5641–5652

Synthesis and Characterization of Novel Fluorinated Poly(oxomolybdates)

Alexej Michailovski,[†] Heinz RUegger,[†] Denis Sheptyakov,[‡] and Greta R. Patzke*[,†]

Laboratory for Inorganic Chemistry, ETH Zürich, CH-8093 Zürich, Switzerland, and Laboratory for Neutron Scattering, ETH Zürich & PSI Villigen, CH-5232 Villigen PSI, Switzerland

Received March 14, 2006

Two novel poly(oxofluoromolybdate) clusters, $[Mo_6O_{18}F_6]^{6-}$ and $[Mo_7O_{22}F_3]^{5-}$, have emerged from systematic field studies on the hydrothermal fluorination of poly(oxometalates). They are accessible via the hydrothermal treatment of Mo(VI)-based precursors in the presence of MF additives (M = Li, Na, Cs, NMe_4). The new fluorinated polyanions are stabilized by specific alkali-cation combinations, and their packing motifs can be tuned through the careful choice of cations and synthetic parameters. The $[Mo_6O_{18}F_6]^{6-}$ anion can be described as a cored and fluorinated form of the Anderson–Evans cluster type. It is stabilized by the interaction of two alkali cations with the fluorinated faces of the ring-shaped anion. The partial replacement of these capping alkali cations by the bulky, organic NMe_4^+ cation leads to the formation of $[Mo_7O_{22}F_3]^{5-}$-based compounds. Thus, the extent of fluorination can be controlled through the polarizability of the cationic environment: in the $[Mo_7O_{22}F_3]^{5-}$ anion, half of the fluoride atoms of the $[Mo_6O_{18}F_6]^{6-}$ anion are replaced by a capping MoO_4 tetrahedron, thereby rendering this anion a fluorinated, lacunar derivative of the α-$[Mo_8O_{26}]^{4-}$ octamolybdate anion. All compounds have been structurally characterized by single-crystal X-ray diffraction and solid-state NMR spectroscopy. The templating role of the alkali cations is discussed and explained with the help of electrostatic calculations.

Introduction

The controlled preparation of new crystalline inorganic solids is a challenging area of research that has much benefited from the recent developments in low-temperature routes.[1] Among these synthetic approaches, solvothermal methods offer an exceptionally wide spectrum of preparative options covering crystal growth techniques, the synthesis of micro- and mesoporous materials, and new pathways to nanoscale compounds.[2] The synthetic parameters (e.g., reactant type or concentration, temperature, pH, etc.) can be widely varied in solvothermal/hydrothermal synthesis, and their effect upon the number and types of phases formed in a given reaction is still difficult to predict.[3,4] Therefore, considerable optimization may be required for the development of a synthetic procedure, and this holds especially true for products that can only be accessed in a narrow window of synthetic parameters.[4,5]

The flexibility of hydrothermal methods renders them ideal for retrieving new compounds among important classes of materials, such as the family of poly(oxomolybdates), which exhibits a diverse structural chemistry.[6] These compounds provide interesting applications (e.g., in catalysis[7] or in

* To whom correspondence should be addressed. E-mail: patzke@inorg.chem.ethz.ch. Phone: +41 44 632 6743. Fax: +41 44 632 1149.

[†] Laboratory of Inorganic Chemistry, ETH Zürich.

[‡] Laboratory for Neutron Scattering, ETH Zürich & PSI Villigen.

(1) (a) Whittingham, M. S.; Guo, J.-D.; Chen, R.; Chirayil, T.; Janauer, G.; Zavalij, P. *Solid State Ionics* **1995**, *75*, 257. (b) Rouxel, J.; Tournoux, M. *Solid State Ionics* **1996**, *84*, 141. (c) Gopalakrishnan, J. *Chem. Mater.* **1995**, *7*, 1265.

(2) (a) Byrappa, K.; Yoshimura, M. *Handbook of Hydrothermal Technology*; Noyes: Park Ridge, NJ, 2001. (b) Rao, C. N. R.; Deepak, F. L.; Gundiah, G.; Govindaraj, A. *Prog. Solid State Chem.* **2003**, *31*, 5. (c) Komarneni, S. *Curr. Sci.* **2003**, *85*, 1730. (d) Demazeau, G. *J. Mater. Chem.* **1999**, *9*, 15. (e) Patzke, G. R.; Krumeich, F.; Nesper, R. *Angew. Chem., Int. Ed.* **2002**, *41*, 2446.

(3) (a) Walton, R. I.; Millange, F.; Smith, R. I.; Hansen, T. C.; O'Hare, D. *J. Am. Chem. Soc.* **2001**, *123*, 12547. (b) Cheetham, A. K.; Mellot, C. F. *Chem. Mater.* **1997**, *9*, 2269.

(4) Michailovski, A.; Krumeich, F.; Patzke, G. R. *Helv. Chim. Acta* **2004**, *87*, 1029.

(5) Michailovski, A.; Willems, J. B.; Stock, N.; Patzke, G. R. *Helv. Chim. Acta* **2005**, *88*, 2479.

(6) (a) Xu, Y. *Curr. Opin. Solid State Mater. Sci.* **1999**, *4*, 133. (b) Clearfield, A. *Prog. Cryst. Growth Charact. Mater.* **1991**, *21*, 1. (c) Pope, M. T., Müller, A., Eds. *Perspectives in the Solid State Coordination Chemistry of the Molybdenum Oxides*; Kluwer Academic Publishers: Dordrecht, The Netherlands, 2001. (d) Rarig, R. S.; Hagrman, P.; Zubieta, J. *Solid State Sci.* **2002**, *4*, 77. (e) Pope, M. T., Müller, A., Eds. *Polyoxometalates: From Platonic Solids to Anti-Retroviral Activity*; Kluwer Academic Publishers: Dordrecht, The Netherlands, 1994.

10.1021/ic0604359 CCC: $33.50
Published on Web 06/15/2006

Table 1. Representative Synthetic Conditions for Hexafluorohexa- and Trifluoroheptamolybdates (Reaction Time = 2 days)

compound	M1:M2	Mo:F	T (°C)	precursor
$Li_2Cs_4Mo_6O_{18}F_6 \cdot 6H_2O$ (**1**)	7:3	1:2	220	ammonium heptamolybdate
$Na_2Cs_4Mo_6O_{18}F_6 \cdot 6H_2O$ (**2**)	4:1	1:2	180	$MoO_3 \cdot 2H_2O$
$Na_2K_4Mo_6O_{18}F_6 \cdot 2H_2O$ (**2a**)	2:3	1:2	180	MoO_3
$Na_2Rb_4Mo_6O_{18}F_6 \cdot nH_2O$ (**2a**)	2:3	1:2	180	MoO_3
$Na_2(NH_4)_4Mo_6O_{18}F_6 \cdot nH_2O$ (**2a**)	4:1	1:2	220	MoO_3
$0.9Na_4(NMe_4)_2Mo_6O_{18}F_6 \cdot 10H_2O \cdot 0.1Na_3(NMe_4)_2Mo_7O_{22}F_3 \cdot 9H_2O$ (**3**)	4:1	1:4	140	MoO_3
m-$Na_2(NMe_4)_3Mo_7O_{22}F_3 \cdot 6H_2O$	3:2	1:2	140	MoO_3
t-$Na_2(NMe_4)_3Mo_7O_{22}F_3 \cdot 6H_2O$	1:4	1:2	140	MoO_3

photochemistry[8]) arising from a broad range of structural motifs.[9] Their dimensionality increases from isolated tetrahedral and octahedral moieties[10] over polyanions[11] and two-dimensional layers[12] to three-dimensional tunnel and network structures.[13] Recently, a new class of giant molybdate clusters with nanoscale dimensions has opened up new perspectives in nanomaterials chemistry.[14]

Generally, the molybdate structure type formed in a given reaction strongly depends on the synthetic conditions, and this makes the development of predictive procedures quite difficult. In the course of our ongoing research on systematic hydrothermal approaches to oxide materials, we have focused on the role of the molybdate precursor material and its interaction with alkali cations to develop synthetic guidelines for controlled access to poly[oxomolybdates(VI)].[4,5] The combination of appropriate alkali-cation pairs with the matching type of Mo-based precursor (e.g., layered materials vs cluster compounds) opens up differentiated pathways to new mixed alkali molybdates and alkali fluoromolybdates. The synthesis of fluoromolybdates adds an interesting "design" approach to the structural chemistry of molybdates, because the fluoride anion can act as a "chemical scissors" by cutting up molybdate layers or chains into smaller fluorinated units.[5,15] However, the number of different fluoromolybdate types is still surprisingly limited, and the majority of them consist either of isolated MoO_xF_y octahedra or of the respective dimers (cf. Table S1 in the Supporting Information). The latter can further be connected to form fluorinated chains (cf. Table S1 in the Supporting Information). $[Mo_xO_yF_z]$ units have been observed in extended structures, e.g., the $\{Mo_2O_4F_2(O_3PR)_2\}$ subunit in $[\{Ni_3(tpyprz)_2(H_2O)_2\}(Mo_5O_{15})(Mo_2O_4F_2)\{O_3P(CH_2)_3PO_3\}_2] \cdot 8H_2O$ (tpyprz = tetra-2-pyridylpyrazine).[16] Up to now, only two fluorinated polymolybdate anions have been characterized: $[Mo_4O_{12}F_2]^{2-}$ and $[Mo_8O_{26}F_2]^{6-}$.[17,18] The former coexists with the hexamolybdate anion, $[Mo_6O_{19}]^{2-}$, in $[Ni(tpyrpyz)_2]_2[Mo_4O_{12}F_2][Mo_6O_{19}] \cdot 2H_2O$.[17] The $[Mo_8O_{26}F_2]^{6-}$ difluorooctamolybdate anion can be understood as a monomer resulting from the fluorination and cleavage of $M_4Mo_8O_{26}$ chain molybdates. $K_6Mo_8O_{26}F_2 \cdot 6H_2O$ has long been the only known difluorooctamolybdate[18] until our systematic hydrothermal studies brought forward new packing motifs in mixed alkali difluorooctamolybdates.[5] These results pointed to a general synthetic trend: the combination of different (alkali) countercations exerts a considerable structure-directing potential on the resulting mixed molybdate.

In this paper, we report on the synthesis and characterization of two new fluoromolybdate types: $(M,M')_6Mo_6O_{18}F_6 \cdot 6H_2O$ (M = Na, Li; M′ = K−Cs, NH_4, NMe_4) and t/m-$Na_2(NMe_4)_3Mo_7O_{22}F_3 \cdot 6H_2O$. They contain the novel fluorinated polyanions $[Mo_6O_{18}F_6]^{6-}$ and $[Mo_7O_{22}F_3]^{5-}$, respectively. In the following, we discuss (a) the hydrothermal parameter windows and the templating role of cation pairs for the formation of the new fluoromolybdates and (b) the key position of the new fluoromolybdate anions in the general context of poly(oxomolybdate) structures.

Experimental Section

Preparative Methods. In a representative solvothermal experiment, precursor material containing 1 mmol of molybdenum (e.g., 180 mg of $MoO_3 \cdot 2H_2O$, synthesized from sodium molybdate and $HClO_4$[19]), 2 mL of H_2O, and alkali/tetramethylammonium fluorides in the appropriate ratio (for further details, compare Table 1) were inserted into a Teflon-lined stainless steel autoclave with a capacity of 23 mL. The sealed autoclave was heated for 2 days at temperatures between 140 and 220 °C, followed by cooling to room temperature. The resulting precipitate was filtered off, washed with distilled H_2O, ethanol, and diethyl ether, and dried in air.

Powder X-ray Diffraction Analysis. Powder diffraction data were collected on a STOE STADI-P2 diffractometer in transmission mode (flat sample holders or 0.1-mm capillaries, germanium-monochromated Cu $K\alpha_1$ radiation) equipped with a position-sensitive detector (resolution of ca. 0.01° in 2θ).

X-ray Data Collection and Structure Determination. Single-crystal X-ray diffraction data were collected on a Bruker AXS SMART CCD diffractometer using Mo Kα radiation (λ = 0.710 73 Å), and the data reduction was performed with the *SAINT* software.[20] The program XPREP[21] was used for space-group determination. The structures were solved by direct methods

(7) (a) Baiker, A.; Dollenmeier, P.; Reller, A. *J. Catal.* **1987**, *103*, 394. (b) Ressler, T.; Wienold, J.; Jentoft, R. E. *J. Catal.* **2002**, *210*, 67.
(8) Yamase, T. *J. Chem. Soc., Dalton Trans.* **1985**, 2585.
(9) Yamase, T.; Pope, M. T. *Polyoxometalate Chemistry for Nanocomposites Design*; Kluwer Academic Publishers: Dordrecht, The Netherlands, 2002.
(10) Gonschorek, W.; Hahn, T. *Z. Kristallogr.* **1973**, *138*, 167.
(11) Bridgeman, A. J. *J. Phys. Chem. A* **2002**, *106*, 12151.
(12) Gatehouse, B. M.; Miskin, B. K. *Acta Crystallogr.* **1975**, *B31*, 1293.
(13) Guo, J.; Zavalij, P.; Whittingham, M. S. *J. Solid State Chem.* **1995**, *117*, 323.
(14) Liu, T.; Diemann, E.; Li, H.; Dress, A. W. M.; Müller, A. *Nature* **2003**, *426*, 59.
(15) Gatehouse, B. M.; Leverett, P. *J. Chem. Soc. A* **1971**, 2107.
(16) Burkholder, E.; Golub, V.; O'Connor, C. J.; Zubieta, J. *Inorg. Chem.* **2004**, *43*, 7014.
(17) Burkholder, E.; Zubieta, J. *Inorg. Chim. Acta* **2004**, *357*, 279.
(18) Kamenar, B.; Kaitner, B.; Strukan, N. *Acta Crystallogr.* **1990**, *C46*, 2249.
(19) Cruywagen, J. J.; Heyns, J. B. B. *S. Afr. J. Chem.* **1981**, *34*, 118.
(20) *SAINT*, version 4.05; Siemens Analytical X-ray Instruments: Madison, WI, 1996.
(21) *SHELXTL*, version 5.1; Program Package; Bruker AXS: Madison, WI.

Table 2. Crystallographic Data for $Li_2Cs_4Mo_6O_{18}F_6 \cdot 6H_2O$ (**1**), $Na_2Cs_4Mo_6O_{18}F_6 \cdot 6H_2O$ (**2**), and $0.9Na_4(NMe_4)_2Mo_6O_{18}F_6 \cdot 10H_2O \cdot 0.1Na_3(NMe_4)_2Mo_7O_{22}F_3 \cdot 9H_2O$ (**3**)

compound	**1**	**2**	**3**
formula	$Cs_4H_{12}F_6Li_2Mo_6O_{24}$	$Cs_2H_6F_3Mo_3NaO_{12}$	$C_4H_{12}F_3Mo_{3.11}Na_{1.85}O_{14}$
fw	1631.19	831.63	695.53
T (K)	295(2)	295(2)	295(2)
λ (Å)	0.71073	0.71073	0.71073
cryst syst	triclinic	monoclinic	triclinic
space group	$P\bar{1}$	$P2_1/n$	$P\bar{1}$
a (Å)	8.076(1)	10.315(1)	8.166(1)
b (Å)	10.272(1)	9.909(1)	11.865(1)
c (Å)	10.417(1)	15.702(2)	11.933(1)
α (deg)	109.63(1)	90.00	108.35(1)
β (deg)	92.34(1)	106.59(1)	97.72(1)
γ (deg)	113.04(1)	90.00	109.64(1)
V (Å^3)	734.1(1)	1538.1(2)	995.5(2)
Z	1	4	2
d_{calcd} (g cm^{-3})	3.663	3.565	2.324
μ (mm^{-1})	7.495	7.183	2.053
no. of param	191	191	253
R1[a]/wR2[b] [$I > 2\sigma(I)$]	0.0350/0.0754	0.0229/0.0457	0.0349/0.0813
R1[a]/wR2[b] (all data)	0.0468/0.0769	0.0373/0.0470	0.0549/0.0875
$\Delta\rho_{max}$ (e Å^{-3})	1.764	1.823	1.027
$\Delta\rho_{min}$ (e Å^{-3})	−1.570	−0.994	−0.789
GOF (F^2)	0.820	0.874	1.027

[a] $R1 = \sum||F_o| - |F_c||/\sum|F_o|$. [b] $wR2 = [\sum\{w(F_o^2 - F_c^2)^2\}/\sum\{w(F_o^2)^2\}]$.

(*SHELXS-97*[21]) and refined against F^2 with the full-matrix least-squares method (*SHELXL-97*[22]). Empirical absorption corrections were performed with the program *SADABS*.[23] The non-hydrogen atoms were located by difference Fourier syntheses and refined anisotropically. Hydrogen atoms were introduced at calculated positions, and they were refined with a riding model. In t-$Na_2(NMe_4)_3Mo_7O_{22}F_3 \cdot 6H_2O$, the aquoligand O24 was refined as a split position. All crystallographic data are summarized in Tables 2, 5, and 6.

Structure Determination from Powder Diffraction Data. The powder pattern of $Na_2K_4Mo_6O_{18}F_6 \cdot 2H_2O$ was indexed in a monoclinic cell with the following dimensions: $a = 15.182(1)$ Å, $b = 9.711(1)$ Å, $c = 9.812(1)$ Å, $\beta = 107.72(2)°$ (Tables 5 and S3 in the Supporting Information). According to the systematic absences, the space group $P2_1/n$ has been assigned. The crystal structure solution has been carried out with the use of the global optimization techniques implemented in the structure solution package FOX.[24] The hexafluorohexamolybdate moiety and the adjacent sodium atoms have been initially put in as a rigid-body object. This was established by putting solely the bond distance constraints at the values close to those observed in $Na_2Cs_4Mo_6O_{18}F_6 \cdot 6H_2O$. The potassium atoms and H_2O molecules were left free to be located independently. Once convergence was achieved, the refinement of the crystal structure parameters was carried out with the use of Fullprof software.[25] The refinement turned out to be so robust that all of the positional parameters of the individual atoms were finally refined independently. A few narrow regions with the peaks of an unidentified impurity had to be excluded from the refinement (Figure S3 in the Supporting Information and Tables 5 and S3 in the Supporting Information). The isotropic temperature factors were constrained to be identical for all atoms, and the refined value amounts to $B_{iso,overall} = 3.08(5)$ Å^2.

Elemental Analyses. The alkali content of selected fluorinated poly(oxomolybdates) was determined on a CamScan CS-44 electron microscope with an EDAX-Phoenix energy-dispersive X-ray spectrometer. Fluorine contents were determined by ion chromatography on a Metrohm 761 Compact IC. C, H, and N analyses were carried out by means of combustion test methods on a LECO CHN-900.

Solid-State NMR Spectroscopy. Solid-state NMR spectra have been recorded at 194.0, 470.6, 132.3, and 65.6 MHz for the isotopes ^{7}Li, ^{19}F, ^{23}Na, and ^{133}Cs, respectively. The compounds were contained in zirconium oxide rotors of 4-mm outer diameter and spun at rotation frequencies of up to 12 kHz in the magic angle. The ^{13}C carboxylate resonance of glycine was used for field calibration, and referencing was then achieved on the absolute frequency scale according to the recommendation of IUPAC.[26] Isotropic chemical shifts or maxima of absorptions for ^{19}F and the quadrupolar nuclei ^{7}Li, ^{23}Na, and ^{133}Cs, respectively, are expressed relative to CCl_3F, LiCl, NaCl, and $CsNO_3$ in solution phase.[26]

Computational Details. The interaction of the cations with the respective poly[oxomolybdate(VI)] frameworks has been investigated with the help of electrostatic models.[27]

As a validation of the structure refinement, the Madelung part of the lattice energy (MAPLE)[28,29] and the atomic point potentials were determined using the program *MADKUG*.[30] All calculations were performed for the ionic limit (2− charge for oxygen, 1− charge for fluorine, 1+ charge for the alkali cations, and 6+ charge for molybdenum). The theoretical MAPLE values were calculated from the sum of the MAPLE values of the binary oxides and fluorides. Note that the calculation of the atomic point potentials is generally more accurate for cations than for anions. However, *all* of our calculations on poly[oxomolybdate(VI)] systems have revealed a common trend: the point potentials of the oxygen atoms increase with their coordination number. μ_1-Oxygen atoms exhibit values (atomic units) of around 1.5−1.9, followed by atomic point potentials between ca. 2.0 and 2.4 for μ_2-oxygen atoms. The values increase to 2.5−2.7 for μ_3-oxygen atoms and finally to atomic point potentials of 2.8 and above for μ_4-oxygen atoms.

The bond valences[31] are calculated via the relation[32]

$$v_{ij} = \exp[(R_0 - d_{ij})/0.37]$$

with R_0 representing the valence bond parameter and d_{ij} the actual distance between two atoms. The bond valence parameters were taken from tabulated R_0 values.[33,34] The bond valence sums (BVSs) are simply obtained by summing over all neighbors at each site.[35,36]

(22) Sheldrick, G. M. *SHELX97, Programs for the Refinement of Crystal Structures*; University of Göttingen: Göttingen, Germany, 1997.
(23) Sheldrick, G. M. *SADABS*; University of Göttingen: Göttingen, Germany, 1997.
(24) Favre-Nicolin, V.; Cerny, R. *J. Appl. Crystallogr.* **2002**, *35*, 734.
(25) Rodríguez-Carvajal, J. *Physica B* **1993**, *192*, 55.
(26) Harris, R. K.; Becker, E. D.; Cabral de Menezes, S. M.; Goodfellow, R.; Granger, P. *Pure Appl. Chem.* **2001**, *73*, 1795.
(27) (a) Hoppe, R. *Angew. Chem.* **1970**, *82*, 7. (b) Hoppe, R.; Bernet, K.; Moeller, A. *Z. Anorg. Allg. Chem.* **2003**, *629*, 1285.
(28) (a) Hoppe, R. *Angew. Chem., Int. Ed. Engl.* **1966**, *5*, 52. (b) Hoppe, R. *Adv. Fluorine Chem.* **1970**, *6*, 387. (c) Weiss, C.; Hoppe, R. *Z. Anorg. Allg. Chem.* **1996**, *622*, 1019.
(29) (a) Hoppe, R. In *Crystal Structure and Chemical Bonding in Inorganic Chemistry*; Rooymans, C. J. M., Rabenau, A., Eds.; North-Holland Publishing Co.: Amsterdam, The Netherlands, 1975; p 127. (b) Lissner, F.; Schleid, T. *Z. Anorg. Allg. Chem.* **1994**, *620*, 1998.
(30) (a) Nesper, R.; Roch, G.; Neukäter, B.; von Schnering, H.-G. *MADKUG, A Program for the Calculation of Lattice Energies, Madelung Factors, and Point Potentials*; Universität Münster: Zürich, Switzerland, 1993. (b) Rohrer, F. E.; Nesper, R. *J. Solid State Chem.* **1998**, *135*, 194.
(31) (a) Brown, I. D.; Altermatt, D. *Acta Crystallogr.* **1985**, *B41*, 240. (b) Brown, I. D.; Altermatt, D. *Acta Crystallogr.* **1985**, *B41*, 244.
(32) (a) Donnay, G.; Allmann, R. *Am. Mineral.* **1970**, *55*, 1003. (b) Adams, S. *Acta Crystallogr.* **2001**, *B57*, 278.
(33) (a) Brese, N. E.; O'Keeffe, M. *Acta Crystallogr.* **1991**, *B47*, 192. (b) García-Rodríguez, L.; Rute-Pérez, A.; Ramón Piñero, J.; González-Silgo, C. *Acta Crystallogr.* **2000**, *B56*, 565.
(34) (a) Brown, I. D. *Acta Crystallogr.* **1976**, *A32*, 24. (b) Brown, I. D. *Acta Crystallogr.* **1976**, *A32*, 786. (c) Brown, I. D.; Wu, K. K. *Acta Crystallogr.* **1976**, *B32*, 1957.

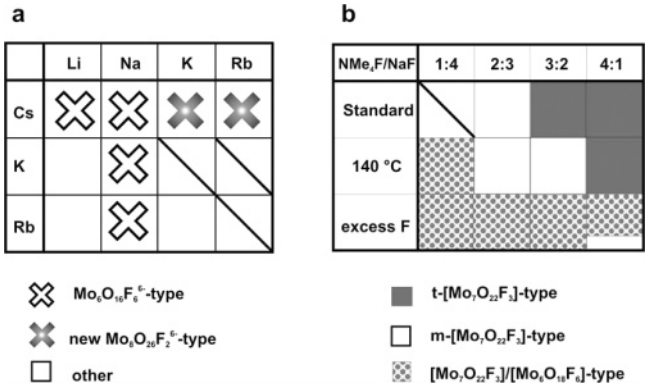

Figure 1. Synthetic parameter fields for the formation of $[Mo_6O_{18}F_6]^{6-}$ hexafluorohexamolybdates (a) and $[Mo_7O_{22}F_3]^{5-}$ trifluoroheptamolybdates (b). Standard procedure = MoO_3, 140 or 180 °C, 2 days, Mo:F = 1:2.

Results and Discussion

Hydrothermal Synthesis of $(M,M')_6Mo_6O_{18}F_6$-Type Hexafluorohexamolybdates. Screening experiments with molybdenum-based precursors and alkali/ammonium fluoride solutions revealed that new mixed alkali fluoromolybdates are preferably formed in the presence of sodium or cesium cations (Figure 1).

Depending on the synthetic parameter window and on the molybdenum-precursor material, three different hexafluorohexamolybdate types containing the new $Mo_6O_{18}F_6^{6-}$ anion are accessible (Table 1). The synthesis of $Li_2Cs_4Mo_6O_{18}F_6 \cdot 6H_2O$ (type 1) is only successful if ammonium heptamolybdate is subjected to 2 days of hydrothermal treatment at 220 °C in a suspension of NaF in an aqueous solution of CsF (molar ratio Li/Cs = 2.3; Table 1). While the Mo/F ratio may be chosen between 0.5 and 0.1, all other parameter changes, especially reaction temperatures below 220 °C, lead to the formation of different products.

$Na_2Cs_4Mo_6O_{18}F_6 \cdot 6H_2O$ (type 2) can be obtained from the treatment of either $MoO_3 \cdot 2H_2O$ or ammonium heptamolybdate in NaF/CsF solutions. The NaF/CsF ratio must be carefully adjusted in the temperature range between 180 and 220 °C, so that the synthetic parameter window remains rather narrow (NaF/CsF = 9 at 180 °C for $MoO_3 \cdot 2H_2O$ and 2.3−9 (180 °C) or 4 (220 °C) for ammonium heptamolybdate). For the preparation of polycrystalline type 2a fluoromolybdates ($Na_2M_4Mo_6O_{18}F_6 \cdot 6H_2O$; M = K, Rb, NH_4), much less optimization work was required. $Na_2K_4Mo_6O_{18}F_6 \cdot 2H_2O$ is accessible from the hydrothermal reaction of all three precursor materials in NaF/KF solutions. $MoO_3 \cdot 2H_2O$ or MoO_3 works best for the quantitative formation of $Na_2K_4Mo_6O_{18}F_6 \cdot 2H_2O$ at a minimum reaction temperature of 180 °C in fluoride solutions with a NaF/KF ratio of 0.66 and above. The same trend applies for the synthesis of $Na_2Rb_4Mo_6O_{18}F_6 \cdot nH_2O$: starting from $MoO_3 \cdot 2H_2O$, it is formed quantitatively at 180−220 °C with NaF/RbF ratios of 0.66 and below. The precursor materials MoO_3 and ammonium heptamolybdate require elevated temperatures (220 °C) or Mo/F ratios lower than 0.5. Finally, $Na_2(NH_4)_4Mo_6O_{18}F_6 \cdot nH_2O$ can easily be prepared from the hydrothermal treatment of any of the three precursors in the temperature window between 180 and 220 °C in NaF/NH_4F solutions (0.25−1.5 ratios). However, considerable optimization efforts could not bring forward any single crystals of type 2a hexafluorohexamolybdates.

Table S2 in the Supporting Information displays representative elementary analyses of all fluoromolybdate types. The experimental results are in good agreement with the expected values.

Hydrothermal Synthesis of $[Mo_7O_{22}F_3]$-Type Trifluoroheptamolybdates. The hydrothermal reaction of MoO_3 or $MoO_3 \cdot 2H_2O$ in NaF/NMe_4F solutions afforded two modifications of $Na_2(NMe_4)_3Mo_7O_{22}F_3 \cdot 6H_2O$ (Table 1) containing the novel $[Mo_7O_{22}F_3]^{5-}$ trifluoroheptamolybdate anion. The latter could only be obtained from the layered precursor materials (MoO_3 and $MoO_3 \cdot 2H_2O$) but not from ammonium heptamolybdate. Higher NMe_4F/NaF ratios favor the formation of triclinic $Na_2(NMe_4)_3Mo_7O_{22}F_3 \cdot 6H_2O$, whereas the monoclinic modification prevails at lower NMe_4F/NaF ratios. Furthermore, the third new fluoromolybdate type compound contains a mixture of $[Mo_6O_{18}F_6]^{6-}$ hexafluorohexamolybdate anions and $[Mo_7O_{22}F_3]^{5-}$ anions, giving rise to the overall formula $(Na_4(NMe_4)_2Mo_6O_{18}F_6 \cdot 10H_2O)_{1-x}(Na_3(NMe_4)_2Mo_7O_{22}F_3 \cdot 9H_2O)_x$ ($x = 0.06-0.44$). The elementary analyses for all trifluoroheptamolybdates (Table S2 in the Supporting Information) agree well with the calculated values.

Crystal Structures. The crystallographic data for all compounds are summed up in Tables 2, 5, and 6. Selected bond lengths and the results of the electrostatic calculations are listed in Tables 3, 4, 7, and 8.

$M_2M'_4Mo_6O_{18}F_6 \cdot 6H_2O$ Hexafluorohexamolybdates (M = Li, Na; M′ = K−Cs, NH_4). The $M_2M'_4Mo_6O_{18}F_6 \cdot 6H_2O$ hexafluorohexamolybdates all have the novel $[Mo_6O_{18}F_6]^{6-}$ anion in common, which consists of six edge-sharing MoO_4F_2 octahedra (Figures 2 and 3).

Each octahedron shares two edges with neighboring octahedra to form a hexagonal ring with idealized D_{3d} symmetry. The fluorine anions are located at its two triangular faces, which are capped by the M-alkali cations, and these fluoromolybdate moieties are surrounded by the M′ cations. Two different packing types of hexafluorohexamolybdates can be accessed through appropriate (M, M′) cation combinations.

$Li_2Cs_4Mo_6O_{18}F_6 \cdot 6H_2O$ (Type 1 Hexafluorohexamolybdate). The triclinic hexafluorohexamolybdate $Li_2Cs_4Mo_6O_{18}F_6 \cdot 6H_2O$ contains lithium-bicapped $[Mo_6O_{18}F_6]$ rings (Figure 3a). The lithium cations are tetrahedrally coordinated to three crystallographically different fluorine atoms and one aquoligand (crystal H_2O) with Li−F bond lengths of 1.876(9)−1.891(9) Å, a Li−O distance of 1.893(9) Å, and bond angles between 105.8(4)° and 111.8(4)° (Tables 3 and 4). The calculated BVS of Li^+ (1.05) is in good agreement with the expected value of 1.00. Figure 4a shows the stacking motif of the lithium-capped rings. The oxygen atoms of the hexafluorohexamolybdate ring can be subdivided into two types: the terminal (μ_1) oxygen atoms (O4−O9) are equally

(35) He, M.; Okudera, H.; Simon, A. *Inorg. Chem.* **2005**, *44*, 4421.
(36) (a) Buttrey, D. J.; Vogt, T.; Yap, G. P. A.; Rheingold, A. L. *Mater. Res. Bull.* **1997**, *7*, 947. (b) Chen, M. D.; Zhou, Z. H.; Hu, S. Z. *Chin. Sci. Bull.* **2002**, *47*, 978.

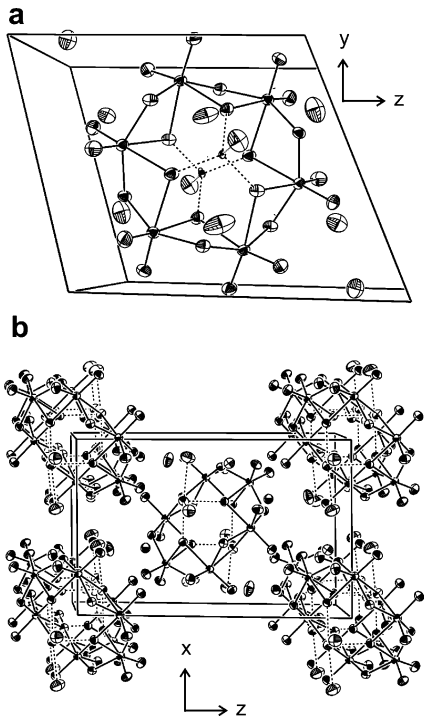

Figure 2. Projection of the unit cell of (a) $Li_2Cs_4Mo_6O_{18}F_6 \cdot 6H_2O$ along [100] and (b) $Na_2Cs_4Mo_6O_{18}F_6 \cdot 6H_2O$ along [010] (ORTEP plots, 70% probability).

distributed among the molybdenum atoms Mo1−Mo3 with bond lengths in the range between 1.694(4) and 1.716(4) Å. Three different bridging (μ_2) oxygen atoms (O1−O3) connect the MoO_4F_2 octahedra with bond lengths of 1.911(4)−1.931(4) Å (Table 3). The corresponding Mo−F distances of the μ_2-fluorine atoms (F1−F3) are noticeably longer [(2.241(3)−2.266(3) Å]. All MoO_4F_2 octahedra are therefore distorted. Their bond angles decrease from the μ_1-O−Mo−μ_1-O angles (∼104°) over the bridging μ_2-O−Mo−μ_1-O angles to the μ_2-O−Mo−F angles (∼72°) at the center of the ring, thereby deviating up to 18° from the ideal value of 90° (Table 3). As the corresponding Mo−O/F bond lengths are increasing (Table 3), the molybdenum atoms are displaced toward the μ_1-oxygen atoms of the MoO_4F_2 octahedra so that their edge lengths vary between 2.469(5) and 2.859(5) Å. The three different shared O···F edges exhibit the shortest distances [2.469(5)−2.474(5) Å], whereas the nonbonding F···F distances at the center of the ring are the longest edges [2.832(5)−2.859(5) Å].

The hexafluorohexamolybdate rings in $Li_2Cs_4Mo_6O_{18}F_6 \cdot 6H_2O$ are interconnected by two crystallographically different cesium cations. Cs1 and Cs2 are surrounded by oxygen atoms in an irregular 8-fold and 10-fold fashion, respectively (for details, compare Table 4 and Figure S1 in the Supporting Information). While Cs1 is underbonded (BVS = 0.85), the BVS value for Cs2 (0.96) is close to the expected value of 1.00 (Table 4). A two-dimensional network of hydrogen-bonding interactions[37] exists between the three crystallographically different H_2O molecules and the oxygen atoms

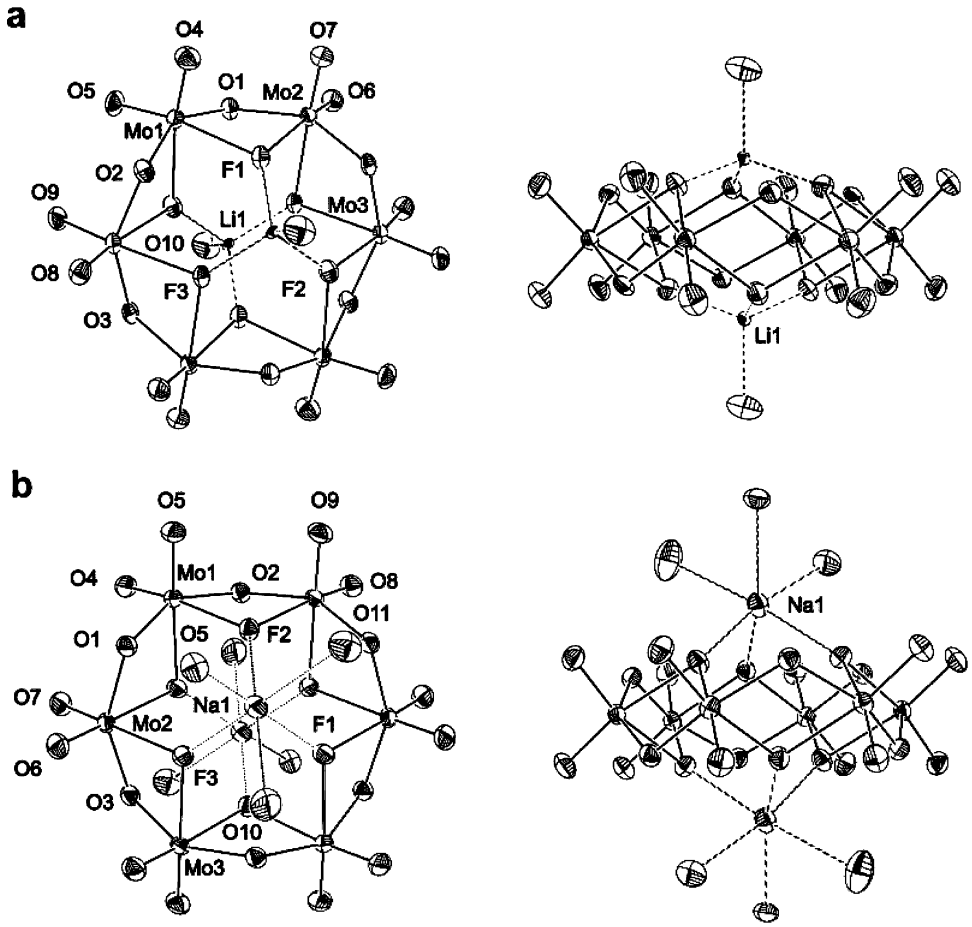

Figure 3. ORTEP views (70% probability thermal ellipsoids) along the 3-fold axis (left) or perpendicular to the 3-fold axis (right) of the $[Mo_6O_{18}F_6]^{6-}$ ring units in $Li_2Cs_4Mo_6O_{18}F_6 \cdot 6H_2O$ (a) and $Na_2Cs_4Mo_6O_{18}F_6 \cdot 6H_2O$ (b).

Table 3. Selected Bond Lengths [Å], Bond Angles [deg], Atomic Point Potentials [au], Bond Valence Sums, and MAPLE Values [kJ mol^{-1}] for the Molybdenum Framework of $[Mo_6O_{18}F_6]^{6-}$-Type Fluoromolybdates

parameter	**1**	**2**	**3**: ring moiety
		Mo−O/F Distance	
μ_1-oxygen	1.694(4)−1.716(4)	1.704(2)−1.713(2)	1.699(2)−1.707(2)
μ_2-oxygen	1.911(4)−1.931(4)	1.922(2)−1.948(2)	1.922(2)−1.944(2)
Mo−F dist.	2.241(3)−2.266(3)	2.208(2)−2.254(2)	2.211(2)−2.262(2)
		Mo−O/F Angle	
μ_2-O−Mo−F	71.7(1)−72.3(1)	71.1(1)−72.4(1)	71.8(1)−72.7(1)
F−Mo−F	77.7(1)−78.7(1)	80.3(1)−82.3(1)	80.7(1)−81.0(1)
μ_2-O−Mo−μ_1-O	99.9(2)−101.7(2)	100.7(1)−101.9(1)	100.7(1)−102.8(1)
μ_1-O−Mo−μ_1-O	104.3(2)−104.7(2)	102.2(1)−102.8(1)	103.6(1)−104.3(1)
		P (O/F)	
μ_1-oxygen	1.750−1.767	1.611−1.949	1.731−1.877
μ_2-oxygen	2.287−2.321	2.296−2.352	2.386−2.449
μ_2-fluorine	1.518−1.548	1.475−1.511	1.609−1.663
		BVS/P (Mo)	
Mo1	6.03/−3.849	5.86/−3.768	5.98/−3.740
Mo2	5.91/−3.837	5.91/−3.884	6.01/−3.769
Mo2	6.03/−3.847	5.93/−3.803	5.97/−3.733
		MAPLE	
calculated	36 812	36 613	36 589
sum (binary)	36 331	36 257	36 393
deviation (%)	+1	+1	+0.5

Table 4. Selected Bond Lengths [Å], Atomic Point Potentials [au], and Bond Valence Sums for the Cationic Part of $[Mo_6O_{18}F_6]^{6-}$-Type Fluoromolybdates

parameter	**1**	**2**	**3**: ring moiety
		M−O/F Distance	
M1−F	1.876(9)−1.891(9)	2.243(2)−2.325(2)	Na1−F: 2.214(2)−2.324(2)
M1−O	1.893(9)	2.400(3)−2.664(3)	Na1−O: 2.335(3)−2.701(3)
Cs1−F	3.789(3)	3.200(2)−3.391(2)	Na2−F: 2.729(3)
Cs1−O	3.189(4)−3.403(4)	3.051(2)−3.391(2)	Na2−O: 2.326(4)−2.514(3)
Cs2−F	3.443(3)	3.372(2)	
Cs2−O	3.064(4)−3.554(6)	2.985(2)−3.333(3)	
		BVS/CN (M)	
M1	1.05/4 (3 F, 1 O)	1.02/6 (3 F, 3 O)	Na1: 1.05/6 (3 O, 3 F)
Cs1	0.85/8	1.25/10 (8 O, 2 F)	Na2: 1.05/6 (5 O, 1 F)
Cs2	0.96/10 (9 O, 1 F)	1.16/9 (8 O, 1 F)	
		P (M)	
M1	−0.458	−0.543	Na1: −0.272
Cs1	−0.903	−0.834	Na2: −0.712
Cs2	−0.849	−0.875	N1: −0.686

of the fluoromolybdate anion including O···O nonbonding distances as short as 2.783(6) Å.

$Na_2Cs_4Mo_6O_{18}F_6\cdot 6H_2O$ (Type 2 Hexafluorohexamolybdate). The $[Mo_6O_{18}F_6]$ rings in $Na_2Cs_4Mo_6O_{18}F_6\cdot 6H_2O$ are bicapped by sodium cations (Figure 3b). The sodium cations are octahedrally coordinated to the three crystallographically different fluorine atoms [Na···F distances between 2.243(2) and 2.325(2) Å], two aquoligands (O10 and O11), and an oxygen atom from a neighboring hexafluorohexamolybdate ring (O5) at elongated Na−O distances between 2.400(3) and 2.664(3) Å. Nevertheless, this leads to a BVS of 1.02 for sodium cations that agrees well with the theoretical value of 1.00. The three-dimensional interconnection of the ring moieties is maintained through the Na1−O5 contact (Figure 4b). The lithium cation in $Li_2Cs_4Mo_6O_{18}F_6\cdot 6H_2O$ is too small to provide a comparable bridging interaction. All Mo−O and Mo−F distances within the sodium-capped hexafluorohexamolybdate ring fall within the ranges observed for $Li_2Cs_4Mo_6O_{18}F_6\cdot 6H_2O$. The introduction of the larger sodium as a capping cation affects the degree of distortion of the MoO_4F_2 octahedra: the nonbonding F···F distances at the center of the ring [2.853(2)−2.953(2) Å] are significantly longer than those in the lithium-capped ring [2.832(5)−2.859(5) Å]. Consequently, the F−Mo−F angles in $Na_2Cs_4Mo_6O_{18}F_6\cdot 6H_2O$ slightly increase with respect to the lithium-containing compound (∼81° vs ∼78°), whereas the μ_1-O−Mo−μ_1-O angles are compressed in the presence of the sodium cation (∼102° vs ∼104°). Compared to $Li_2Cs_4Mo_6O_{18}F_6\cdot 6H_2O$, the interconnection of the rings through hydrogen bonding in $Na_2Cs_4Mo_6O_{18}F_6\cdot 6H_2O$ is weaker [nonbonding O···O distances between 2.817(3) and 2.906(3) Å]. As observed in $Li_2Cs_4Mo_6O_{18}F_6\cdot 6H_2O$, the sodium-containing hexafluorohexamolybdate rings are interconnected by two crystallographically different cesium cations (Figure 4), Cs1 and Cs2 (for details, compare Table 4 and Figure S2 in the Supporting Information). Cs1 is surrounded by six oxygen atoms and two fluorine atoms of the molecular rings together with two additional aquoligands, thereby exhibiting an irregular 10-fold coordination. The most striking difference between the cesium positions in $Li_2Cs_4Mo_6O_{18}F_6\cdot 6H_2O$ and $Na_2Cs_4Mo_6O_{18}F_6\cdot 6H_2O$ is the significant increase in the BVS for Cs1 (1.25) and Cs2 (1.16) in the sodium-based compound.

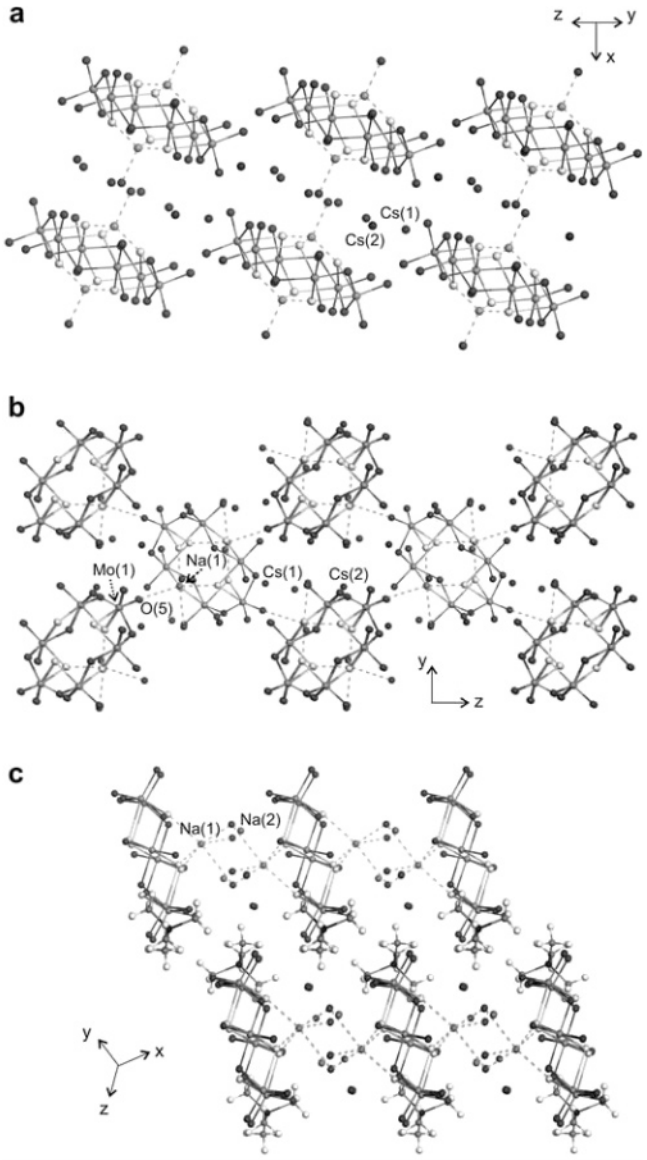

Figure 4. Packing motifs of the $[Mo_6O_{18}F_6]^{6-}$ units in $Li_2Cs_4Mo_6O_{18}F_6 \cdot 6H_2O$ (a), $Na_2Cs_4Mo_6O_{18}F_6 \cdot 6H_2O$ (b), and $0.9Na_4(NMe_4)_2Mo_6O_{18}F_6 \cdot 10H_2O \cdot 0.1Na_3(NMe_4)_2Mo_7O_{22}F_3 \cdot 9H_2O$ (c).

This overbonding of both cations might be related to the close O−Na−O bridging of the ring units in $Na_2Cs_4Mo_6O_{18}F_6 \cdot 6H_2O$ (Figure 4b): the large cesium cations have to fit into this sodium-templated, three-dimensional network of molecular rings.

$Na_2M_4Mo_6O_{18}F_6 \cdot nH_2O$ (M = K, Rb, NH_4; Type 2a Hexafluorohexamolybdates). Contrary to the type 1 and 2 hexafluorohexamolybdates, the isostructural $Na_2M_4Mo_6O_{18}F_6 \cdot nH_2O$ (M = K, Rb, NH_4) hexafluorohexamolybdate series exhibits considerable difficulties in crystal growth. Despite numerous optimization experiments, no single crystals could be obtained so that a structural model was developed for $Na_2K_4Mo_6O_{18}F_6 \cdot 2H_2O$ on the basis of powder diffraction data and solid-state NMR data for $Na_2(NH_4)_4Mo_6O_{18}F_6 \cdot nH_2O$ that support the presence of hexafluorohexamolybdate anions in the type 2a compounds (compare the Experimental Section and below). The summary of the crystallographic parameters of $Na_2K_4Mo_6O_{18}F_6 \cdot 2H_2O$ is given in Tables 5 and S3 in the Supporting Information. $Na_2K_4Mo_6O_{18}F_6 \cdot 2H_2O$ and $Na_2Cs_4Mo_6O_{18}F_6 \cdot 6H_2O$ display identical packing motifs of the hexafluorohexamolybdate moieties (compare Figure 4b) so that the $Na_2M_4Mo_6O_{18}F_6 \cdot nH_2O$ (M = K, Rb, NH_4) compounds have been assigned as the type 2a series.

Table 5. Crystallographic Data for $Na_2K_4Mo_6O_{18}F_6 \cdot 2H_2O$

compound	$Na_2K_4Mo_6O_{18}F_6 \cdot 2H_2O$
formula	$F_6H_4K_4Mo_6Na_2O_{20}$
fw	607.99
T (K)	295(1)
λ (Å)	1.5406
cryst syst	monoclinic
space group	$P2_1/n$
V (Å^3)	1377.8(1)
a (Å)	15.182(1)
b (Å)	9.711(1)
c (Å)	9.812(1)
γ (deg)	107.72(2)
Z	4
d_{calcd} (g cm^{-3})	2.931
χ^2	3.72
R_p	0.0578
R_{wp}	0.0744

$(Na_4(NMe_4)_2Mo_6O_{18}F_6 \cdot 10H_2O)_{1-x}(Na_3(NMe_4)_2Mo_7O_{22}F_3 \cdot 9H_2O)_x$ (0.06 < x < 0.44; Type 3 Fluoromolybdate). The NaF/NMe_4F/MoO_3 hydrothermal system brought forward a mixed triclinic hexafluorohexamolybdate $Na_4(NMe_4)_2Mo_6O_{18}F_6 \cdot 6H_2O$ with the characteristic sodium-bicapped $[Mo_6O_{18}F_6]$ ring (Figure 3b) as the major component. However, electron density plots revealed the presence of two weak maxima close to the peak arising from Na1 (the stronger one is displayed in Figure S4 in the Supporting Information). We have interpreted this phenomenon as a Mo−O bond: thus, a part of the ring anions is capped by sodium on the one side and by a tetrahedral MoO_4 unit on the opposite side of the ring, thereby forming the novel $[Mo_7O_{22}F_3]^{5-}$ fluoromolybdate anion (Figures 5 and 6; for structural details, compare the next section). The $[Mo_7O_{22}F_3]/[Mo_6O_{18}F_6]$ ratio in the products increases with the NMe_4F/NaF ratio in the starting material, and the following discussion is focused on the $Na_4(NMe_4)_2Mo_6O_{18}F_6 \cdot 10H_2O$ part (x = 0.1) of the mixed type 4 fluoromolybdate (compare Table 2 for crystallographic details). As can be seen from Figure 4c, the stacking motif of the molybdate rings is different from the type 1 and 2 fluoromolybdates. The capping sodium cation Na1 is octahedrally coordinated by three fluorine atoms and three aquoligands. Two of the latter are shared with a neighboring Na1 so that the molecular units are connected into chains that are terminated by the capping MoO_4 units. The BVS value of Na1 (1.05) agrees well with the expected value of 1.00. The distorted octahedral environment of Na2 consists of two oxygen atoms and one fluorine atom from the same ring, together with three aquoligands. Na2 does not contribute to electrostatic interactions between different fluoromolybdate moieties, and its BVS is close to unity (1.05; Table 4). The crystal H_2O molecules are engaged in hydrogen bonding with both each other and the fluoromolybdate rings, resulting in O···O distances in the range between 2.707(4) and 2.981(6) Å.

(37) Chippindale, A. M.; Brech, S. J. *J. Chem. Soc., Chem. Commun.* **1996**, 2781.

Table 6. Crystallographic Data for t-$Na_2(NMe_4)_3Mo_7O_{22}F_3{\cdot}6H_2O$ (**1**) and m-$Na_2(NMe_4)_3Mo_7O_{22}F_3{\cdot}6H_2O$ (**2**)

compound	**1**	**2**
formula	$C_{12}H_{36}F_3Mo_7N_3Na_2O_{28}$	$C_{24}H_{72}F_6Mo_{14}N_6Na_4O_{56}$
fw	1445.00	2890.00
T (K)	295(2)	295(2)
λ (Å)	0.71073	0.71073
cryst syst	triclinic	monoclinic
space group	$P\bar{1}$	$C2/c$
a (Å)	11.763(1)	19.141(5)
b (Å)	11.856(1)	13.982(3)
c (Å)	17.058(2)	32.214(8)
α (deg)	108.66(1)	90.00
β (deg)	93.99(1)	99.47(1)
γ (deg)	106.43(1)	90.00
V (Å^3)	2128.0(4)	8504(4)
Z	2	4
d_{calcd} (g cm^{-3})	2.255	2.257
μ (mm^{-1})	2.116	2.118
no. of param	500	498
R1[a]/wR2[b] [$I > 2\sigma(I)$]	0.0425/0.0808	0.0364/0.0847
R1[a]/wR2[b] (all data)	0.0856/0.0945	0.0535/0.0901
$\Delta\rho_{max}$ (e Å^{-3})	0.724	1.169
$\Delta\rho_{min}$ (e Å^{-3})	−0.626	−0.779
GOF (F^2)	0.997	1.048

[a] $R1 = \sum||F_o| - |F_c||/\sum|F_o|$. [b] $wR2 = [\sum\{w(F_o^2 - F_c^2)^2\}/\sum\{w(F_o^2)^2\}]$.

Table 7. Selected Bond Lengths [Å], Angles [deg], and Atomic Point Potentials [au] for the Molybdenum Framework of $[Mo_7O_{22}F_3]^{5-}$-Type Fluoromolybdates

parameter	**1**	**2**
	Mo−O/F Distance	
μ_1-oxygen atoms	1.681(5)−1.711(5)	1.690(4)−1.718(4)
μ_2-oxygen atoms	1.908(5)−1.942(4)	1.916(4)−1.951(4)
μ_3-oxygen atoms	1.782(4)−2.398(4)	1.795(4)−2.369(4)
Mo−F distance	2.225(4)−2.254(3)	2.232(3)−2.260(3)
	Mo−O/F Angle	
μ_2-O−Mo−F	72.1(2)−72.5(2)	71.9(1)−72.5(1)
μ_2-O−Mo−μ_3-O	71.5(2)−72.2(2)	71.3(1)−72.3(1)
μ_3-O−Mo−F	78.0(1)−78.9(1)	77.9(1)−78.9(1)
μ_2-O−Mo−μ_1-O	100.4(2)−103.5(2)	100.2(2)−103.7(2)
μ_1-O−Mo−μ_1-O	103.9(2)−104.5(2)	103.6(2)−105.2(2)
μ_1-O−Mo7−μ_3-O	107.8(2)−111.3(2)	107.5(2)−111.6(2)
	P (O/F)	
μ_1-oxygen atoms	1.721−2.031	1.720−1.941
μ_2-oxygen atoms	2.404−2.463	2.394−2.517
μ_3-oxygen atoms	2.829−2.870	2.831−2.845
μ_2-fluorine	1.657−1.755	1.664−1.762

$Na_2(NMe_4)_3Mo_7O_{22}F_3{\cdot}6H_2O$ Trifluoroheptamolybdates. The two different modifications of $Na_2(NMe_4)_3Mo_7O_{22}F_3$ (triclinic and monoclinic; compare Tables 6−8 and Figures 5−7 and S5 in the Supporting Information) contain the novel $[Mo_7O_{22}F_3]^{5-}$ anion. It is accessible in the temperature window between 140 and 180 °C, starting from MoO_3 as a precursor material (for further details, compare Table 1). The $[Mo_7O_{22}F_3]^{5-}$ anion consists of six MoO_5F octahedra that are connected via alternating O···O and O···F edges into a ring moiety. The ring is almost planar, and the three fluorine atoms at one side are capped by a sodium cation (Figure 5). On the opposite, nonfluorinated side of the ring, the capping position is occupied by a tetrahedral MoO_4 unit (Figure 6 a). As a result, the anion exhibits idealized C_{3v} symmetry (Figure 5).

m-$Na_2(NMe_4)_3Mo_7O_{22}F_3{\cdot}6H_2O$. In the monoclinic modification of $Na_2(NMe_4)_3Mo_7O_{22}F_3{\cdot}6H_2O$ (Figure S5b in the Supporting Information and Figure 7b), the capping sodium cation (Na1) is octahedrally coordinated by the three fluorine atoms of the $[Mo_7O_{22}F_3]^{5-}$ ring and three aquoligands. Na2

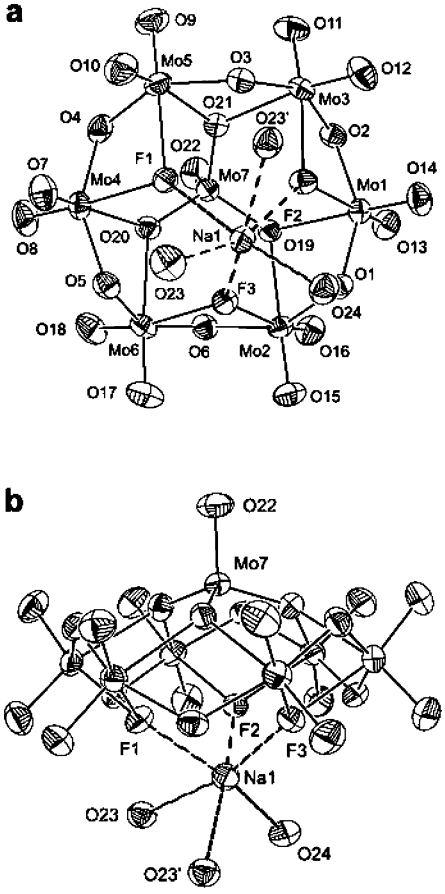

Figure 5. ORTEP views of the $[Mo_7O_{22}F_3]^{5-}$ anion in m-$Na_2(NMe_4)_3$-$Mo_7O_{22}F_3{\cdot}6H_2O$ along (a) and perpendicular (b) to the 3-fold axis (70% probability thermal ellipsoids).

Table 8. Selected Bond Lengths [Å], Bond Valence Sums, Atomic Point Potentials [au], and MAPLE Values [kJ mol^{-1}] for the Cationic Part of $[Mo_7O_{22}F_3]^{5-}$-Type Fluoromolybdates

parameter	**1**	**2**
	M−O/F Distance	
Na1−F	2.268(4)−2.380(4)	2.266(4)−2.363(4)
Na1−O	2.380(5)−2.630(5)	2.369(4)−2.649(5)
Na2−F	2.721(5)	2.690(4)
Na2−O	2.324(8)−2.70(3)	2.327(7)−2.568(6)
	BVS/CN (M)	
Na1	1.00/6 (3F, 3O)	1.01/(3F, 3O)
Na2	0.98/6 (5O, 1F, 1O)	1.01/(5O, 1F)
	Point Potentials	
Na1	−0.195	−0.182
Na2	−0.677	−0.660
N1	−0.685	−0.692
N2	−0.695	−0.702
N3	−0.658	N3: −0.713/N4: −0.608
	BVS/P (Mo)	
Mo1	6.06/−3.773	6.00/−3.725
Mo2	6.02/−3.731	5.98/−3.794
Mo3	5.99/−3.779	5.89/−3.712
Mo4	6.02/−3.804	6.03/−3.794
Mo5	6.08/−3.808	6.05/−3.778
Mo6	6.06/−3.762	5.94/−3.789
Mo7	5.90/−3.381	5.80/−3.389
	MAPLE	
calculated	42 762	42 768
sum of binary compds	41 923	41 923
deviation (%)	+2	+2

is surrounded by one fluorine atom and two μ_1-oxygen atoms of the trifluoroheptamolybdate ring (Figure 5). Three aquoligands complete its strongly distorted octahedral coordination sphere, and the aquoligand O24 is shared with Na1 so

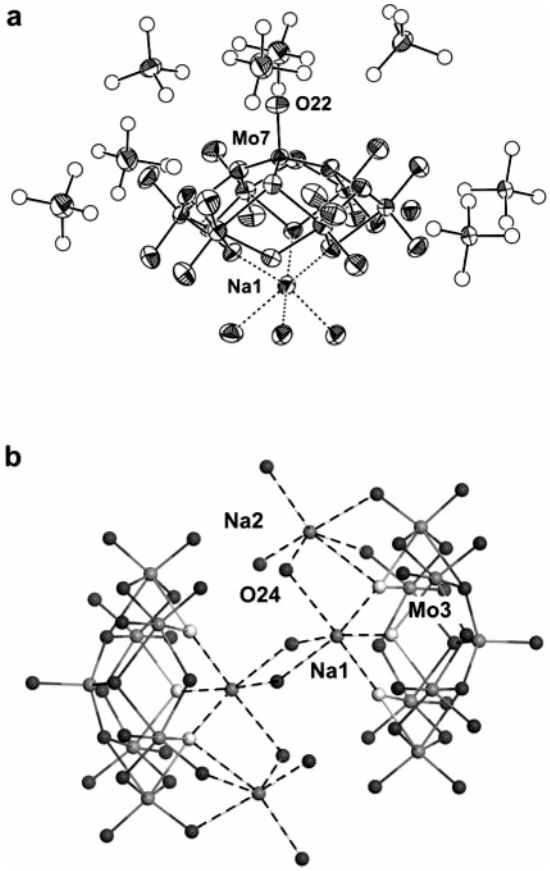

Figure 6. Coordinative environments of the unpolar (a) and polar (b) faces of the $[Mo_7O_{22}F_3]^{5-}$ anion in m-$Na_2(NMe_4)_3Mo_7O_{22}F_3{\cdot}6H_2O$.

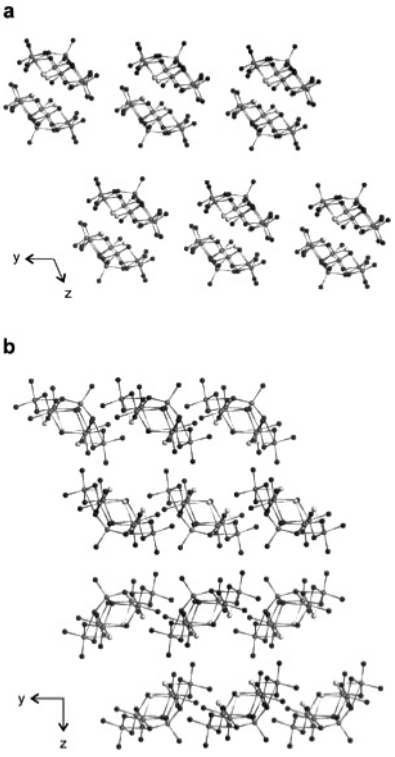

Figure 7. Packing motif of the $[Mo_7O_{22}F_3]^{5-}$ anions in t-$Na_2(NMe_4)_3Mo_7O_{22}F_3{\cdot}6H_2O$ (a) and m-$Na_2(NMe_4)_3Mo_7O_{22}F_3{\cdot}6H_2O$ (b) (the cations have been omitted for clarity).

that the polar fluorinated faces of the molecular rings are connected via a network of sodium cations and crystal H_2O molecules (Figure 6b). All Na−O and Na−F distances are within the expected ranges (compare reference data in Tables 3 and 4), and the BVS values for both Na1 and Na2 are close to unity (Table 8). Both the Mo−O/Mo−F distances of the μ_1- and μ_2-oxygen atoms and of the μ_2-fluorine atoms to the six octahedrally coordinated molybdenum atoms (Table 7) and the trend among the bond angles in the distorted MoO_5F octahedra are analogous to the type 1 and 2 hexafluorohexamolybdates (compare Tables 3 and 7). The capping tetrahedron is distorted so that the Mo7−O bond angles [107.5(2)−111.6(2)°] deviate from the expected value of 109.5°. Whereas the polar, fluorinated sides of two ring moieties are connected via the capping sodium cation Na1 together with Na2 and additional aquoligands, the MoO_4 tetrahedron at the nonfluorinated side of the ring is surrounded by four organic tetramethylammonium cations (Figure 6). They separate the alternating double layers of ring pairs in both modifications (Figure 7).

t-$Na_2(NMe_4)_3Mo_7O_{22}F_3{\cdot}6H_2O$. The triclinic modification of $Na_2(NMe_4)_3Mo_7O_{22}F_3{\cdot}6H_2O$ arises from a different packing motif of the $[Mo_7O_{22}F_3]^{5-}$ anions (Figures 7a and S5 in the Supporting Information). It contains an AAAA... stacking sequence of anion pairs, while the monoclinic modification exhibits an ABABAB... layer sequence (Figure 7b).

While all Mo−O and Mo−F distances of the molecular ring are in the same range as observed for the monoclinic modification (Table 7), there is a noteworthy difference between both modifications regarding the coordinative environment of the sodium cations: the aquoligand O24 that is associated with Na2 had to be refined as a split position (compare Figure 6b). This points to a strain in the bridging arrangement of the sodium cations between the $[Mo_7O_{22}F_3]^{5-}$ rings. As a consequence, the BVS of Mo3 increases from 5.89 in the monoclinic form to 5.99 in the triclinic modification. Furthermore, all BVS values for octahedrally coordinated molybdenum atoms are close to the ideal value of 6.00, and the BVS of the tetrahedrally coordinated Mo7 rises from 5.79 in the monoclinic form to 5.90 in the triclinic form (Table 8).

MAPLE Calculations. The MAPLE values and point potentials for hexa- and heptafluorohexamolybdates are listed in Tables 3, 4, and 8. Generally, a good agreement between the theoretical and calculated MAPLE values has been obtained with an average deviation of 1.3%. This outperforms our previous results on poly[oxomolybdates(VI)] with deviations up to 4%. The calculated point potentials for μ_1- and μ_2-oxygen atoms are within the expected ranges (compare Tables 3 and 7), and the point potentials for the μ_2-fluorine atoms exhibit considerably lower values (1.475−1.762; compare Tables 3 and 7). As expected, all point potentials for the octahedrally coordinated molybdenum atoms are around +3.8. The cationic point potentials in the type 1 and 2 hexafluoromolybdates exhibit substantial differences: the values for both cesium cations in $Li_2Cs_4Mo_6O_{18}F_6{\cdot}6H_2O$ are approximately twice as large as the point potential of the capping lithium (−0.903/−0.849 vs −0.458; Table 4). The trends in $Na_2Cs_4Mo_6O_{18}F_6{\cdot}6H_2O$ are analogous to $Li_2Cs_4Mo_6O_{18}F_6{\cdot}6H_2O$, so that the point potential of Na1 in

the capping position (−0.543) differs considerably from the values for the cesium ions that are located between the fluoromolybdate rings (−0.834/−0.875; Table 4).

The calculated MAPLE value for the $Na_4(NMe_4)_2Mo_6O_{18}F_6 \cdot 10H_2O$ part of the type 3 fluoromolybdates differs by only 0.5% from the theoretical value (Table 3). Concerning the cationic point potentials, the approximate 1:2 ratio between values for the capping cation and for the remaining cationic positions is confirmed (compare sections on type 1 and 2 fluoromolybdates and Table 4).

The MAPLE calculations for t- and m-$Na_2(NMe_4)_3Mo_7O_{22}F_3 \cdot 6H_2O$ deviate by 2% from the expected theorectical value (Tables 7 and 8). Given that all tetramethylammonium cations have been approximated as nitrogen atoms with a uniform 1+ charge, this is still a reasonably good agreement. The point potentials for the six octahedrally coordinated molybdenum atoms are perfectly in line with the values calculated for the hexafluorohexamolybdates (Table 3).

Solid-State NMR Spectroscopy. Poly[oxofluoromolybdates(VI)] were investigated by solid-state NMR spectroscopy using the magic-angle-spinning technique to improve spectral resolution.

^{19}F NMR Spectroscopy. Each crystallographically independent fluorine site gives rise to one resonance whose features are mostly determined by the chemical shift and dipolar interactions. The former leads under the condition of magic angle spinning (MAS) to a resonance line at the position of the isotropic chemical shift accompanied by a set of sidebands separated by the spinning frequency covering approximately the range of the chemical shift anisotropy. The latter, dipolar, interaction is averaged to zero under the experimental conditions.

Consistent with the crystallographically determined structures for $Li_2Cs_4Mo_6O_{18}F_6 \cdot 6H_2O$, $Na_2Cs_4Mo_6O_{18}F_6 \cdot 6H_2O$ and t-$Na_2(NMe_4)_3Mo_7O_{22}F_3 \cdot 6H_2O$, one finds in each case three well-resolved resonances (see Figure 8), whose isotropic chemical shifts are compiled in Table 9. It is of interest to note that signals are found below and above −180 ppm for the lithium and sodium compounds, respectively. The chemical shift anisotropies are quite similar, equal within experimental error, for all sites and can be characterized with their span $\Omega = 110(5)$ and skew $\kappa = 0.30(4)$. The similarity is in agreement with a common structural feature; i.e., all have the same coordination environment. For the compound $Na_2(NH_4)_4Mo_6O_{18}F_6 \cdot nH_2O$, no structural data are available, but its solid-state ^{19}F NMR spectrum (compare Figure 8) shows that its molecular structure must be closely related to those of the other compounds.

^{23}Na and ^{133}Cs NMR Spectroscopy. The resonances for these two isotopes are mostly determined by chemical shift, quadrupolar, and dipolar magnetic interactions. Whereas the chemical shift interaction averages to its isotropic value and the dipolar interaction to zero under MAS, the quadrupolar interaction cannot be averaged to the isotropic value of zero under these conditions and affect the shape and position of the resonance lines. Therefore, we quote in Table 9 the position of the maximum rather than its true chemical shift.

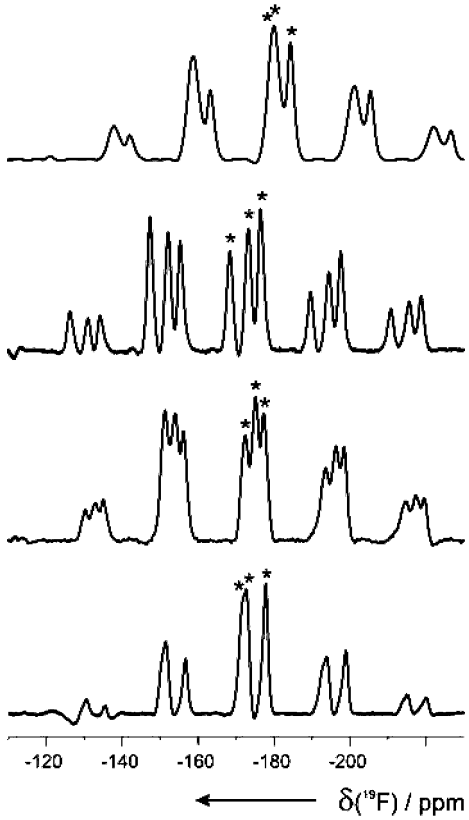

Figure 8. Solid-state 470.6-MHz ^{19}F MAS NMR spectra of $Li_2Cs_4Mo_6O_{18}F_6 \cdot 6H_2O$, $Na_2Cs_4Mo_6O_{18}F_6 \cdot 6H_2O$, $Na_2(NH_4)_4Mo_6O_{18}F_6 \cdot 6H_2O$, and t-$Na_2(NMe_4)_3Mo_7O_{22}F_3 \cdot 6H_2O$ (from top to bottom) recorded at a spinning frequency ν_{rot} of 10 kHz. The isotropic resonance lines are marked with asterisks, and the intensities of the flanking spinning sidebands indicate the chemical shift anisotropies, $\Omega = 110(5)$ and $\kappa = 0.30(4)$. Distortions in the baseline are due to suppression of a large background signal.

Table 9. Solid-State NMR Data[a]

compound	^{7}Li[b]	^{19}F[c]	^{23}Na[b]	^{133}Cs[b]
$Li_2Cs_4Mo_6O_{18}F_6 \cdot 6H_2O$	−0.7	−180.0, −180.0, −184.4		−19, −50
$Na_2Cs_4Mo_6O_{18}F_6 \cdot 6H_2O$		−168.3, −173.2, 176.5	−11.7	47, 25
$Na_2(NH_4)_4Mo_6O_{18}F_6 \cdot nH_2O$		−172.4, −175.1, −177.3	−7.4	
t-$Na_2(NMe_4)_3Mo_7O_{22}F_3 \cdot 6H_2O$		−171.8, −173.2, −176.5	−4.1, −9.1	

[a] Recorded at $B_0 = 11.75$ T under MAS at $\nu_{rot} = 10$ kHz. [b] Position of the maximum of the resonance line on the δ scale. [c] Isotropic chemical shift δ_{iso}.

The expected two sodium resonances in $Na_2Cs_4Mo_6O_{18}F_6 \cdot 6H_2O$, $Na_2(NH_4)_4Mo_6O_{18}F_6 \cdot nH_2O$, and t-$Na_2(NMe_4)_3Mo_7O_{22}F_3 \cdot 6H_2O$ are not well resolved. Only in the last case do two signals seem to be present; however, it cannot completely be excluded that this arises from a quadrupolar effect. Resolution is much better in the ^{133}Cs NMR spectra (Figure 9), where, in agreement with the structural results, two resonances are clearly discernible.

In conclusion, it can be stated that the solid-state NMR spectra are in full agreement with the results from the X-ray structure determination and suggest that the ammonium derivative $Na_2(NH_4)_4Mo_6O_{18}F_6 \cdot nH_2O$ (type 2a) is structurally closely related to the other type 2 hexafluorohexamolybdates.

Structural Relations among Poly[oxofluoromolybdates-(VI)]. The novel ring-shaped $[Mo_6O_{18}F_6]^{6-}$ anions are closelyrelated to α-octamolybdates[38] as well as to $[H_6MMo_6O_{24}]^{n-}$ (M = Al, Cr, Zn, Cu, Co, Ni, Pt, etc.) hexamolybdates[39,40]

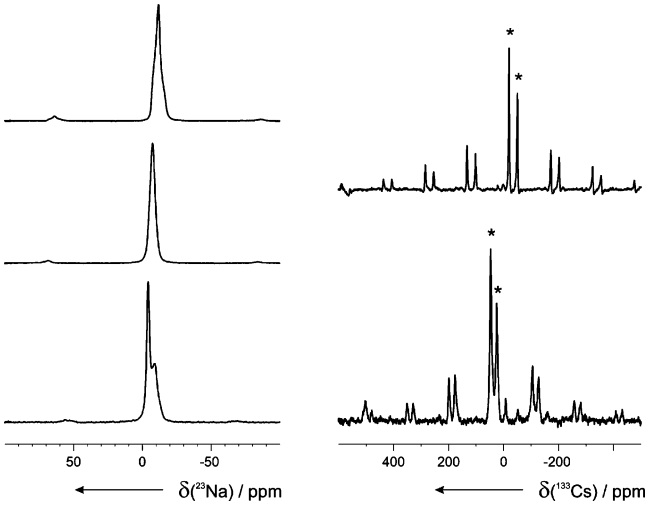

Figure 9. Left: Solid-state 132.3-MHz ^{23}Na MAS NMR spectra of $Na_2Cs_4Mo_6O_{18}F_6 \cdot 6H_2O$, $Na_2(NH_4)_4Mo_6O_{18}F_6 \cdot nH_2O$, and t-$Na_2(NMe_4)_3Mo_7O_{22}F_3 \cdot 6H_2O$ (from top to bottom) recorded at a spinning frequencies ν_{rot} of 10, 10, and 8 kHz, respectively. Note that distinct Na sites are not clearly resolved. Right: Solid-state 65.6-MHz ^{133}Cs MAS NMR spectra of $Li_2Cs_4Mo_6O_{18}F_6 \cdot 6H_2O$ and $Na_2Cs_4Mo_6O_{18}F_6 \cdot 6H_2O$ (from top to bottom) recorded at a spinning frequency ν_{rot} of 10 kHz. Two independent Cs sites are clearly distinguishable.

of the Anderson−Evans type.[41,42] The latter anion with idealized D_{3d} symmetry consists of a central MO_6 octahedron that is surrounded by six edge-sharing MoO_6 units. Six hydrogen atoms are attached to the central oxygen atoms coordinating the metal ion (Figure 10d).

The incorporated heterocation is essential to the stability of the six-membered ring, and an empty $[H_6Mo_6O_{24}]^{6-}$ cluster has never been reported. Instead, the nonplanar $[Mo_6O_{19}]^{2-}$ Lindqvist-type anion represents the stable arrangement of six MoO_6 octahedra into a symmetrical cluster with a 6-fold-coordinated oxygen atom in the center.[43] The newly synthesized $[Mo_6O_{18}F_6]^{6-}$ ring can be described as an empty Anderson−Evans cluster with the central OH units replaced by fluorine atoms (Figure 10c). To the best of our knowledge, this anion is the closest derivative of the hypothetical planar $[H_6Mo_6O_{24}]^{6-}$ cluster that has been reported up to now. Nevertheless, the coordination of small alkali cations (lithium and sodium) to the fluorine atoms is essential to the stability of the $[Mo_6O_{18}F_6]^{6-}$ anion (Figure 10c).

Recently, an interesting new type of "zero-dimensional" telluromolybdates, $A_4Mo_6Te_2O_{24} \cdot 6H_2O$ (A = Rb, K), has been reported. These poly(oxomolybdates) contain flat, hexagonal Mo_6O_{24} rings that are capped by tellurium on both sides so that they can be derived from the Anderson−Evans compounds as well.[44]

Given that the Anderson−Evans-type clusters readily incorporate a variety of transition-metal heteroatoms, we have attempted to generate their fluorinated analogues by introducing Ni^{2+} and Co^{2+} in our solvothermal protocol (compare the Experimental Section). However, all experiments failed to generate the desired compounds of the $[F_6MMo_6O_{18}]^{4-}$ type (M = Co, Ni). As outlined above, single crystals of the type 2a hexafluorohexamolybdates are extremely difficult to obtain. Surprisingly, the presence of Co^{2+} and Ni^{2+} improved the crystallinity of the type 2a compounds without any incorporation reactions or even residual amounts to be detected in the final product so that the according metal fluoride particles might provide additional crystal seeds.

Apart from the Anderson−Evans compounds, the α-octamolybdate anion, α-$[Mo_8O_{26}]^{4-}$, also bears a close resemblance to both new anion types because of its planar ring of six edge-sharing MoO_6 octahedra that is bicapped by two MoO_4 tetrahedra (Figure 10a).[45] The $[Mo_7O_{22}F_3]^{5-}$ anion can therefore be derived from the α-$[Mo_8O_{26}]^{4-}$ anion via the substitution of one MoO_4 tetrahedron by three fluorine atoms capped by a sodium atom (Figure 10b).

Structure−Synthesis Relationships among the Novel Poly[oxofluoromolybdates(VI)]. The narrow parameter windows for the formation of the novel $[Mo_6O_{18}F_6]$ and $[Mo_7O_{22}F_3]$ poly(oxofluoromolybdates) were tracked down through a hydrothermal strategy based on our previous studies on the formation of new $(M,M')_6Mo_8O_{26}F_2$ (M, M′ = K−Cs, NH_4) difluorooctamolybdates. They have revealed that the combination of two different cations (especially Cs/M pairs) triggers the arrangement of the clusters into new packing motifs.[5] This cationic templating potential has been explored in a three-step sequence.

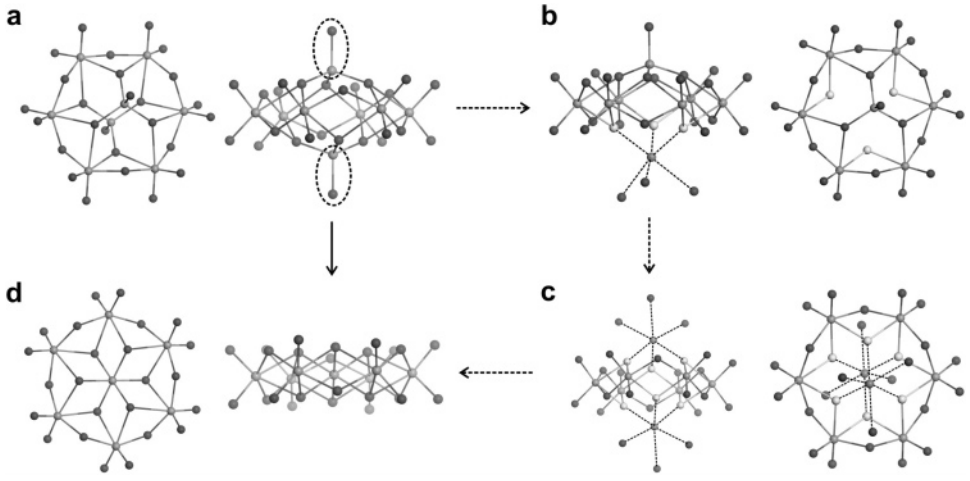

Figure 10. Structural relationships between the α-$[Mo_8O_{26}]^{4-}$ anion (a), the new $[Mo_7O_{22}F_3]^{5-}$ and $[Mo_6O_{18}F_6]^{6-}$ anions (b and c), and the Anderson−Evans clusters (d).

Step 1: Extensive hydrothermal screenings of CsF combined with the fluorides of the smallest alkali cations (LiF and NaF) brought forward the $M_2M'_4Mo_6O_{18}F_6 \cdot 6H_2O$ (M = Li, Na; M′ = Cs) hexafluorohexamolybdates (types 1 and 2).

Step 2: The formation of the type 2a hexafluorohexamolybdate series ($Na_2M_4Mo_6O_{18}F_6 \cdot nH_2O$; M = K, Rb, NH_4) indicated that not only cesium but also sodium is essential for the formation of new fluoromolybdates.

Step 3: Consequently, the combination of sodium with cations larger than cesium was scanned, and the NaF/NMe_4F system brought forward the t/m-$Na_2(NMe_4)_3Mo_7O_{22}F_3 \cdot 6H_2O$ trifluoroheptamolybdates. However, the templating potential of the countercations must be balanced carefully to access a new structure type: when the slightly larger organic NEt_4 cation is employed, its tendency toward the stabilization of nonfluorinated clusters is more pronounced.

The type 3 fluoromolybdates $[(Na_4(NMe_4)_2Mo_6O_{18}F_6 \cdot 10H_2O)_{1-x}(Na_3(NMe_4)_2Mo_7O_{22}F_3 \cdot 9H_2O)_x$ $(0.06 < x < 0.44)]$ demonstrate how the Mo/O/F framework adopts to the changing polarizability of the cationic environment: x increases with the NMe_4F/NaF ratio in the initial composition of the starting materials.

Furthermore, the structure of the molybdenum-based precursor must be taken into consideration. Generally, the layered precursor materials, such as MoO_3 and $MoO_3 \cdot 2H_2O$, have proven more effective in the synthesis of the new fluoromolybdates than the cluster-containing educt ammonium heptamolybdate. Whereas the layered starting materials readily afford all types of the new fluoromolybdates, the heptamolybdate precursor inhibits the formation of the $[Mo_7O_{22}F_3]^{5-}$ heptamolybdates.[5]

Among the remaining synthetic parameters, the MF/M′F ratio, as well as the appropriate choice of the reaction temperature, is of particular importance (e.g., type 3 fluoromolybdates). The reaction time, however, can be more freely chosen, and variations of ±1 days usually do not affect the course of the reaction. Detailed kinetic studies are underway.

Conclusions

Two new classes of fluoromolybdates(VI) have been accessed through hydrothermal parameter studies investigating the reaction of a molybdenum(VI)-based precursor material in alkali and tetramethylammonium fluoride solutions. The alkali fluoride-based systems brought forward three different types of $(M,M')_2Mo_6O_{18}F_6 \cdot nH_2O$ (M = Li, Na; M′ = K−Cs, NH_4; $n = 2-6$) hexafluorohexamolybdates. They have the planar $[Mo_6O_{18}F_6]^{6-}$ anion in common: its fluorinated faces are capped by the smaller M cation, and it can be interpreted as a cored and fluorinated derivative of the Anderson−Evans-type hexamolybdates ($[H_6MMo_6O_{24}]^{n-}$ [M = (transition-) metal cation)]. The degree of fluorination of the Mo/O framework can be reduced in the presence of a bulky organic cation. This results in the formation of the t- and m-$Na_2(NMe_4)_3Mo_7O_{22}F_3 \cdot 6H_2O$ modifications. Both modifications contain the new $[Mo_7O_{22}F_3]^{5-}$ anion that can be understood as a $[Mo_6O_{18}F_6]^{6-}$ anion with one fluorinated face replaced by a capping MoO_4 tetrahedron.

Two main synthetic guidelines can be derived from the hydrothermal screening experiments:

(a) The structure-directing effect of cation combinations with a noticeable difference in ionic radii can be combined with the "chemical scissors" features of fluorine anions. This approach is useful for the directed synthesis of new molybdate frameworks.

(b) Extensive parameter scans (including precursor material, time, and temperature) may still be required to target the narrow synthetic windows of the novel compounds.

All in all, the results illustrate how hydrothermal strategies are perfectly suited to track down previously unknown compounds in molybdate synthesis. Therefore, our ongoing research on poly(oxofluoromolybdates) is now focused on mechanistic in situ studies to gather key information for the first steps toward a real "design" approach.

Acknowledgment. We thank Prof. Dr. R. Nesper (Laboratory of Inorganic Chemistry, ETH Zürich) for his steady interest and for the continuous support of this work. This work was supported by the ETH Zurich, by the Swiss National Science Foundation (MaNEP, Materials with Novel Electronic Properties), and by the National Research Program "Supramolecular Functional Materials".

Supporting Information Available: X-ray crystallographic files of $Li_2Cs_4Mo_6O_{18}F_6 \cdot 6H_2O$, $Na_2Cs_4Mo_6O_{18}F_6 \cdot 6H_2O$, $0.9Na_4(NMe_4)_2Mo_6O_{18}F_6 \cdot 10H_2O \cdot 0.1Na_3(NMe_4)_2Mo_7O_{22}F_3 \cdot 9H_2O$, and t/m-$Na_2(NMe_4)_3Mo_7O_{22}F_3 \cdot 6H_2O$ (CIF), Figures S1−S5, and Tables S1−S3. This material is available free of charge via the Internet at http://pubs.acs.org.

IC0604359

(38) (a) Fuchs, J.; Hartl, H. *Angew. Chem., Int. Ed. Engl.* **1976**, *15*, 15. (b) Hsieh, C. T.; Shaikh, S. N.; Zubieta, J. *Inorg. Chem.* **1999**, *38*, 4480. (c) Day, V. W.; Friedrich, M. F.; Klemperer, W. G.; Shum, W. *J. Am. Chem. Soc.* **1977**, *99*, 952.

(39) (a) Perloff, A. *Inorg. Chem.* **1970**, *9*, 2228. (b) Allen, C. C.; Burns, R. C.; Lawrance, G. A.; Turner, P.; Hambley, T. W. *Acta Crystallogr.* **1997**, *C53*, 7. (c) Lee, H. Y.; Park, K. M.; Lee, U.; Ichida, H. *Acta Crystallogr.* **1991**, *C47*, 1959. (d) Drewes, D.; Krebs, B. *Z. Anorg. Allg. Chem.* **2005**, *631*, 2591.

(40) (a) Ito, F.; Ozeki, T.; Ichida, H.; Miyame, H.; Sasaki, Y. *Acta Crystallogr.* **1989**, *C45*, 946. (b) Lee, U.; Joo, H.-C.; Kwon, J.-S.; Cho, M.-A. *Acta Crystallogr.* **2001**, *E57*, i112. (c) Lee, U.; Joo, H.-C.; Kwon, J.-S. *Acta Crystallogr.* **2002**, *E58*, i6. (d) Lee, U. *Acta Crystallogr.* **1994**, *C50*, 1657.

(41) Anderson, J. S. *Nature (London)* **1937**, *140*, 850.

(42) Evans, H. T., Jr. *J. Am. Chem. Soc.* **1948**, *70*, 1291.

(43) Lindqvist, L. *Ark. Kemi* **1950**, *2*, 325.

(44) Balraj, V.; Vidyasagar, K. *Inorg. Chem.* **1998**, *37*, 4764.

(45) Klemperer, W. G.; Shum, W. *J. Am. Chem. Soc.* **1976**, *98*, 8291.